Acta Metallurgica Sinica (English Letters) (2019) 32:719–725
https://doi.org/10.1007/s40195-018-0830-5

Superparamagnetic $CoFe_2O_4$@Au with High Specific Absorption Rate and Intrinsic Loss Power for Magnetic Fluid Hyperthermia Applications

Sandip Sabale[1,2] · Vidhya Jadhav[2] · Shubhangi Mane-Gavade[2] · Xiao-Ying Yu[1]

Received: 15 May 2018 / Revised: 27 July 2018 / Published online: 10 October 2018

Abstract
$CoFe_2O_4$ nanoparticles (NPs) and surface modified with gold (Au) have been synthesized by a thermal decomposition method. The obtained NPs and formation of $CoFe_2O_4$@Au core–shell (CS) were confirmed by characterizing their structural and optical properties using X-ray powder diffraction (XRD) patterns, Fourier transform infrared spectroscopy, Raman spectroscopy, UV–Visible and photoluminescence studies. Morphological and compositional studies were carried out using high-resolution transmission electron microscopy and energy-dispersive X-ray spectroscopy, while the magnetic properties were determined using alternating gradient magnetometer and Mossbauer to define the magneto-structural effects of shell formation on the core NPs. Induction heating properties of $CoFe_2O_4$ and $CoFe_2O_4$@Au CS magnetic nanoparticles (MNPs) have been investigated and correlated with magneto-structural properties. Specific absorption rate and intrinsic loss power were calculated for these MNPs within the human tolerable range of frequency and amplitude, suggesting their potential in magnetic fluid hyperthermia therapy for possible cancer treatment.

Keywords $CoFe_2O_4$@Au · Superparamagnetic · Specific absorption rate (SAR) · Intrinsic loss power (ILP) · Magnetic fluid hyperthermia

1 Introduction

Magnetic nanoparticles (MNPs), especially superparamagnetic iron oxide nanoparticles (SPIONs), have shown to have potential for use in biomedical applications such as in targeted drug delivery, imaging, magnetic fluid hyperthermia (MFH) and biosensors [1–3]. The ability of SPIONs to convert the electromagnetic energy into heat is the main reason for SPION-based biomedical applications. This heat generation technique by SPION mediators plays an important role in cancer treatment with hyperthermia and multimodal imaging [4, 5]. Recently, MNP-based MFH proved more therapeutically efficient than the common chemotherapeutic drugs (i.e., doxorubicin and Feridex) [6]. Different types of SPIONs have been studied for their effectiveness as hyperthermia agents [3]. These SPIONs are either magnetite (Fe_3O_4) or maghemite (γ-Fe_2O_3), stabilized by coating with a variety of ligands such as dextran, cationic liposomes, polyvinyl alcohol, lauric acid and oleic acid [3]. Another category of these SPIONs is the metal-doped ferrites, MFe_2O_4, (M = Co^{2+}, Mn^{2+}, Ni^{2+}, Zn^{2+}, Mg^{2}) [7–9]. Biomedical applications for such MNPs have been limited so far due to their instability under physiological conditions, harmful free radical formation and inappropriate surface binding of the ligand. In particular, SPIONs are cytotoxic to different types of cells because of Fe-induced intracellular formation of reactive oxygen species as Fe seeps into the cellular milieu [3]. Cytotoxicity arises due to the absence of biocompatible or protective coating which prevents the seepage of Fe from SPIONS surfaces. Hence, coating with biocompatible

Available online at http://link.springer.com/journal/40195

Electronic supplementary material The online version of this article (https://doi.org/10.1007/s40195-018-0830-5) contains supplementary material, which is available to authorized users.

✉ Sandip Sabale
srsabale@gmail.com

✉ Xiao-Ying Yu
xiaoying.yu@pnnl.gov

[1] Earth and Biological Sciences Directorate, PNNL, Richland, WA 99352, USA

[2] Department of Chemistry, Jaysingpur College Jaysingpur, Shivaji University, Kolhapur, MS 416101, India

materials like polymers, organic agents, metal oxides and metals (e.g., Au, Ag and noble metals) resulting in core@shell (CS) can impart significant protection against the Fe-mediated toxicity [3, 10–12].

Of particular interest, Au coating over SPIONs leads to its promising properties such as low reactivity and biocompatibility, thereby making them important in in vivo studies. The positive interaction of thiol-type functional groups and surface plasmon resonance (SPR) contributes to drug delivery and imaging; hence, the SPIONs@Au CS plays a dual modality application as diagnostics and therapeutic agents [4, 13]. Therefore, researchers have focused their attention on the formation of Au shell on the SPIONs. The effectiveness of coating depends on many factors including synthesis methods and in situ formation pathways of Au shell [2, 10]. Moreover, applications related to hyperthermia cancer treatment depend on the overall size, magnetic properties, specific absorption rate (SAR) and intrinsic loss power (ILP) values of the SPIONs. Compared with magnetite/maghemite, $CoFe_2O_4$ NPs present improved magnetic properties due to their high relaxivity and magnetic anisotropy, and are useful in hyperthermia treatment [3]. So far, no reports have shown the synthesis and induction heating studies of $CoFe_2O_4$@Au CS for hyperthermia applications in cancer treatment.

The aim of this work is to synthesize biocompatible $CoFe_2O_4$@Au CS. Herein, we report the simple, fast and one-pot synthesis of superparamagnetic $CoFe_2O_4$ and $CoFe_2O_4$@Au CS MNPs by the complex decomposition method with significant improvement over previously reported methods [7, 14]. The obtained MNPs were characterized and explored for induction heating studies at different applied AC magnetic fields, from which the SAR and ILP values were determined to find out the possible potential of the obtained $CoFe_2O_4$@Au CS MNPs.

2 Experimental

The $CoFe_2O_4$ and $CoFe_2O_4$@Au CS MNPs were prepared by complex decomposition method. Briefly, a solution of $Co(acac)_2$ (2 mmol), $Fe(acac)_3$ (4 mmol), oleylamine (6 mmol), oleic acid (6 mmol) in mixture of diethylene glycol and ethylene glycol (10 mL each) was purged with N_2 for 10 min at 120 °C with stirring. Solution was then refluxed at 210 °C for 2 h followed by cooling; 15 mL solution was taken out as $CoFe_2O_4$, and remained solution was used as it is for the synthesis of $CoFe_2O_4$@Au MNPs. The washing and separation are done as per procedure explained in Supplementary materials. A solution of $HAuCl_4{\cdot}3H_2O$ (0.339 g), oleylamine (1.5 mL), oleic acid (1 mL) in mixture of diethylene glycol and ethylene glycol (2.5 mL each) was purged with N_2 for 5 min with stirring. The obtained gold solution was slowly added to the $CoFe_2O_4$ solution with constant stirring and purging with N_2. The resulting solution is then refluxed at 180 °C for 1.5 h and cooled at room temperature. Washing and separation steps were followed (in Supplementary materials). The UV absorption spectrum was recorded for washings to check the removal of Au NPs, and it is confirmed that no Au is removed from washings which supports the conversion of all gold precursors to form $CoFe_2O_4$@Au. Finally obtained MNPs were dispersed in toluene and dried by washing with ethanol at the time of characterization as powder. The obtained MNPs and formation of CS were confirmed by characterizing their structural properties using XRD, FTIR and Raman spectroscopy, and optical properties using UV–Visible and photoluminescence studies. Morphological and compositional studies were carried out using HRTEM and EDX, while the magnetic properties were determined using M–H curves and Mossbauer to define the magneto-structural effect of shell formation on the core NPs. The obtained MNPs and CSs were explored for induction heating studies to determine the applicability needed in hyperthermia therapy (Supplementary materials). Specific absorption rate (SAR) and intrinsic loss power (ILP) were determined to explain the heating properties of the obtained MNPs. We provide a simple and practical method for high-throughput synthesis of MNPs suitable in hyperthermia treatment.

3 Results and Discussion

The XRD patterns of $CoFe_2O_4$ (red) and $CoFe_2O_4$@Au (blue) NPs are compared in Fig. 1a. The XRD pattern of $CoFe_2O_4$ NPs showed the diffraction peaks at 30.16°, 35.34°, 42.97°, 56.31° and 62.41° of 2θ, corresponding to the peak indices 220, 311, 400, 333 and 440, respectively, while the presence of additional peaks of Au in $CoFe_2O_4$@Au CSs at 38.28°, 44.48°, 64.68° and 77.88° attributed to peak indices 111, 200, 220 and 311, thus confirming the formation of $CoFe_2O_4$@Au CSs [15]. However, the peaks for $CoFe_2O_4$ in CSs are slightly suppressed when compared to the XRD pattern of $CoFe_2O_4$ alone. This is most likely caused by the higher electron density from Au due to the formation of Au coating on the $CoFe_2O_4$ NPs. This effect has been observed previously, providing further evidence of the presence of Au in the NPs [14, 16]. The absence of 210 and 300 peaks confirms the phase purity of the obtained ferrite. The XRD patterns also validate the formation of a spinel phase cubic ferrite with space group *Fd3m*. The crystallite sizes were determined using Scherer's formula [7], which shows the increase in the size (Table 1) of $CoFe_2O_4$ (4.8 nm) by $\sim$ 1 nm, leading to the formation of $CoFe_2O_4$@Au (5.9 nm). The spinel ferrite

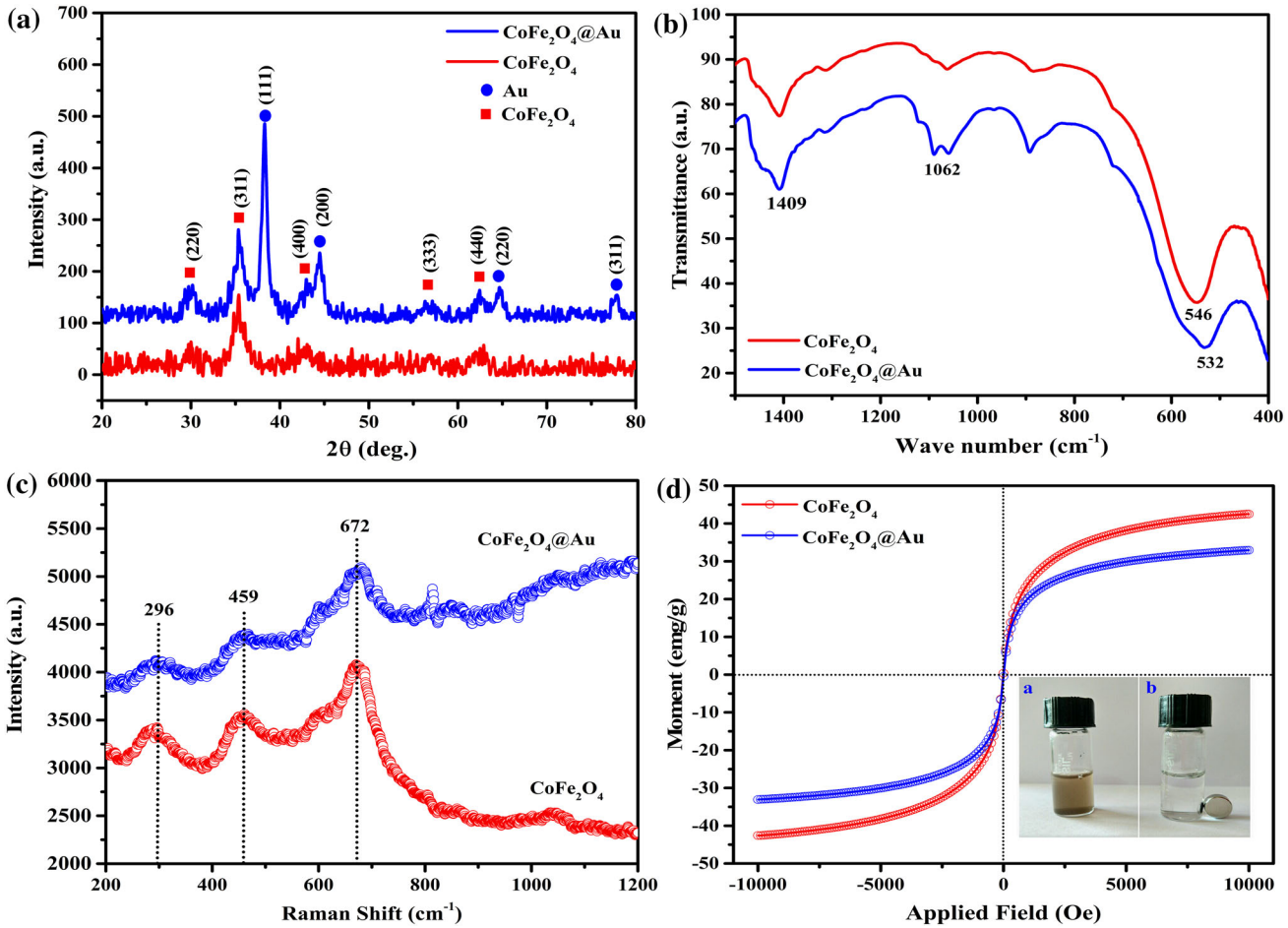

Fig. 1 Structural, optical and magnetic properties of $CoFe_2O_4$NPs (red) and $CoFe_2O_4$@Au CSs (blue) NPs. X-ray diffraction pattern **a** (filled blue circles and red square showing the representative peaks for Au and $CoFe_2O_4$ in core–shell pattern); infrared absorption spectra **b**; Raman spectra showing the Raman active bands excited at 488 nm **c**; room temperature *M–H* curves **d** (the inset shows the $CoFe_2O_4$@Au CSs suspension before **a**, after **b** an external magnetic field)

Table 1 Summary of the crystallite size from XRD (D_{XRD}), TEM diameter (D_{TEM}), saturation magnetization (M_S), coercivity (H_C), composition from EDS analysis, average isomer shift (I_S) and internal hyperfine field (H_f) from Mossbauer analysis of obtained MNPs

Sample	D_{XRD} (nm)	D_{TEM} (nm)	M_S (emu g^{-1})	H_C (Oe)	Composition (wt%)				I_S (mm s^{-1})	H_f (mm s^{-1})
					O	Fe	Co	Au		
$CoFe_2O_4$	4.8 ± 0.83	4.50 ± 0.5	42.59	7.65	21.87	50.75	27.37	–	0.373 ± 0.041	31.6 ± 1.40
$CoFe_2O_4$@Au	5.9 ± 0.35	5.10 ± 0.5	33.02	0.0	21.18	41.77	22.74	14.31	0.328 ± 0.028	26.6 ± 1.10

formation was further supported by the FTIR spectra [15, 17] (Fig. 1b; S2). It is worth noting that the intense and broad absorption bands at 546 cm^{-1} and 532 cm^{-1} were observed for the $CoFe_2O_4$ and $CoFe_2O_4$@Au NPs corresponding to the Fe–O and Co–O (metal–oxide) vibrational stretch in the spinel ferrite, respectively. Furthermore, the observed shift in the band value in the CSs is attributed to the formation of the thin shell of Au. The Raman active bands observed near 296 cm^{-1}, 459 cm^{-1} and 672 cm^{-1} in our work (Fig. 1c) are generally similar to those observed in the literature [18, 19]. The intense band at 672 cm^{-1} (682 cm^{-1}) is assigned to the A_{1g} symmetry (tetrahedral site), and the band at 459 cm^{-1} (470 cm^{-1}) is characteristic of the octahedral site that indicates the absence of magnetite, hence the phase purity of $CoFe_2O_4$. The difference in the intensity ratio of the Raman peaks at 672 and 459 cm^{-1} confirms the presence of octahedrally coordinated Co^{2+}. The relative intensities of Raman active bands

in the $CoFe_2O_4$@Au CSs were found to be lower due to Au coating (Fig. 1c), proving the formation of pure phase $CoFe_2O_4$ NPs and supporting the presence of Au on its surface.

The UV–Visible absorption spectra of the pure $CoFe_2O_4$ (red) and $CoFe_2O_4$@Au (blue) NPs were depicted in Fig. S1 (Supplementary materials). No absorption peak was exhibited in the spectrum of $CoFe_2O_4$ NPs. However, $CoFe_2O_4$@Au CSs showed a clear SPR broadband which appeared in the visible–NIR region with the formation of nanoshell by Au NPs attachment to $CoFe_2O_4$ NPs [20]. The absence of the sharp absorption peak at 520 nm supports the removal of individual Au NPs from the particles. The shell formation is also evidenced by the photoluminescence spectra (in Fig. S3 of Supplementary materials). The characteristic emission peak of Au NPs was observed at 778 nm [21] which illustrated the presence of Au on $CoFe_2O_4$ NPs. The saturation magnetization (M_S) obtained for $CoFe_2O_4$ NPs and $CoFe_2O_4$@Au CSs (Fig. 1d) was 42.59 and 33.02 emu g^{-1}, respectively (Table 1), which showed a decrease in the M_S value due to the formation of Au nonmagnetic thin shell on the surface of $CoFe_2O_4$. The remanence or coercivity (H_C) of $CoFe_2O_4$ and $CoFe_2O_4$@Au CSs was found to be very low (7.65 Oe) and almost zero, respectively, due to the combination of Au and the oleylamine capping shell on the $CoFe_2O_4$ NPs. These magnetic properties depict the superparamagnetic behavior of the obtained MNPs. Hence, the thin Au coating is expected to exert less effect on the magnetic behavior of $CoFe_2O_4$ NPs. To determine the effect of coating Au on the magnetism behavior of MNPs, the ^{57}Fe Mossbauer measurements were conducted in constant acceleration mode. The spectra are found to be very broad for both samples, indicating the distribution of hyperfine fields. Hence, the data were analyzed with the distribution of hyperfine fields using the NORMOS/DIST program (Fig. 2a, b). The obtained hyperfine parameters are shown in Table 1. Figure 2a, b shows that the fit hyperfine distribution gives a sextet with a similar full-width half-maxima (FWHM) (0.45 mm s^{-1}) in both cases, which is the characteristic property of the superparamagnetic $CoFe_2O_4$ core [22]. The slight decrease in the average isomer shift (0.045 mm s^{-1}) and internal hyperfine field (5 mm s^{-1}) is the consequence of the shell in the CSs case as observed by the *M–H* curves. The existence of the strong inter-particle interactions as a result of the high magnetization, fine nanoparticle size and the relaxation effects showed a broad hyperfine distribution with a sextet in Mossbauer analysis. These interactions were also evident from the aggregation of the particles, as observed from HRTEM micrographs of $CoFe_2O_4$ (Fig. 2c, d) and $CoFe_2O_4$@Au (Fig. 2e, f). The TEM micrographs depict a quasi-spherical morphology with a size of 4.50 ± 0.5 and 5.10 ± 0.5 nm for bare and core@shell NPs, respectively. The values are consistent with the crystallite size obtained from XRD patterns. The $CoFe_2O_4$@Au appears darker than the $CoFe_2O_4$ NPs because of the heavy atom effect of Au as seen in the HRTEM image [23]. The compositional analysis determined by energy-dispersive X-ray spectroscopy (EDS) (Table 1) indicates the existence of Fe, O, Co and Au elements in the core–shell sample. The low intensities of Au peaks at 2.2 keV and 8–10 keV in the EDS spectra (Figs. S4 and S5 of Supplementary materials) indicate the presence of Au with an ultra-thin shell on the surface of $CoFe_2O_4$ [16]. All of the above results support the formation of the phase pure inverse spinel ferrite with a cubic structure $CoFe_2O_4$ NPs and subsequent core–shell formation with an ultra-thin layer (i.e., $\sim$ 1 nm) of Au.

To define the applicability and the effect of the coating of Au on the performance of $CoFe_2O_4$ for hyperthermia applications, these NPs and CS were further explored within induction heating studies. Heating properties of the obtained MNPs in this work were determined from the temperature as a function of time with different AC magnetic fields and at a frequency of 276 kHz as shown in Fig. 3a, b ($CoFe_2O_4$ NPs) and Fig. 3c, d ($CoFe_2O_4$@Au CSs). The heating ability of the NPs was then determined from the initial slope of the rise in temperature curves in terms of SAR values (Supplementary materials). The amplitude of the magnetic field and frequency requirements are satisfied in our study (details in Supplementary materials). The time-dependent temperature curves showed that 5 mg mL^{-1} $CoFe_2O_4$ NPs (Fig. 3a) and $CoFe_2O_4$@Au CSs (Fig. 3c) attain a threshold hyperthermia temperature value (> 41 °C) within a similar time period. On the other hand, the increase in the concentration to 10 mg mL^{-1} decreases the time for $CoFe_2O_4$ NPs (Fig. 3b), while it takes more time for $CoFe_2O_4$@Au CSs (Fig. 3d) to reach the threshold temperature. The field amplitude 13.3 kA m^{-1} is not sufficient for 5 and 10 mg mL^{-1} $CoFe_2O_4$ NPs and also for 5 mg mL^{-1} $CoFe_2O_4$@Au CSs. Overall, the threshold temperature can be obtained in less time with an increase in the amplitude of the AC magnetic field. The maximum temperature rise (ΔT) was determined in terms of the amplitude (Table 2), showing a maximal value at 26.7 kA m^{-1}. $CoFe_2O_4$ NPs can produce a maximal ΔT of 25.89 and 35.43 °C; while $CoFe_2O_4$@Au CSs produce 27.94 and 31.10 °C for 5 and 10 mg mL^{-1}, respectively, at 26.7 kA m^{-1}. As expected, values of ΔT and SAR (Table 2) for $CoFe_2O_4$ NPs were greater than those of $CoFe_2O_4$@Au CSs. This increase may be assigned to higher magnetization observed in the case of $CoFe_2O_4$ NPs when compared to CSs. The nonmagnetic property of Au reduces inter-particle interactions, thereby affecting the temperature rise. The presence of Au on the surface of $CoFe_2O_4$ also affects the anisotropy of particles, which

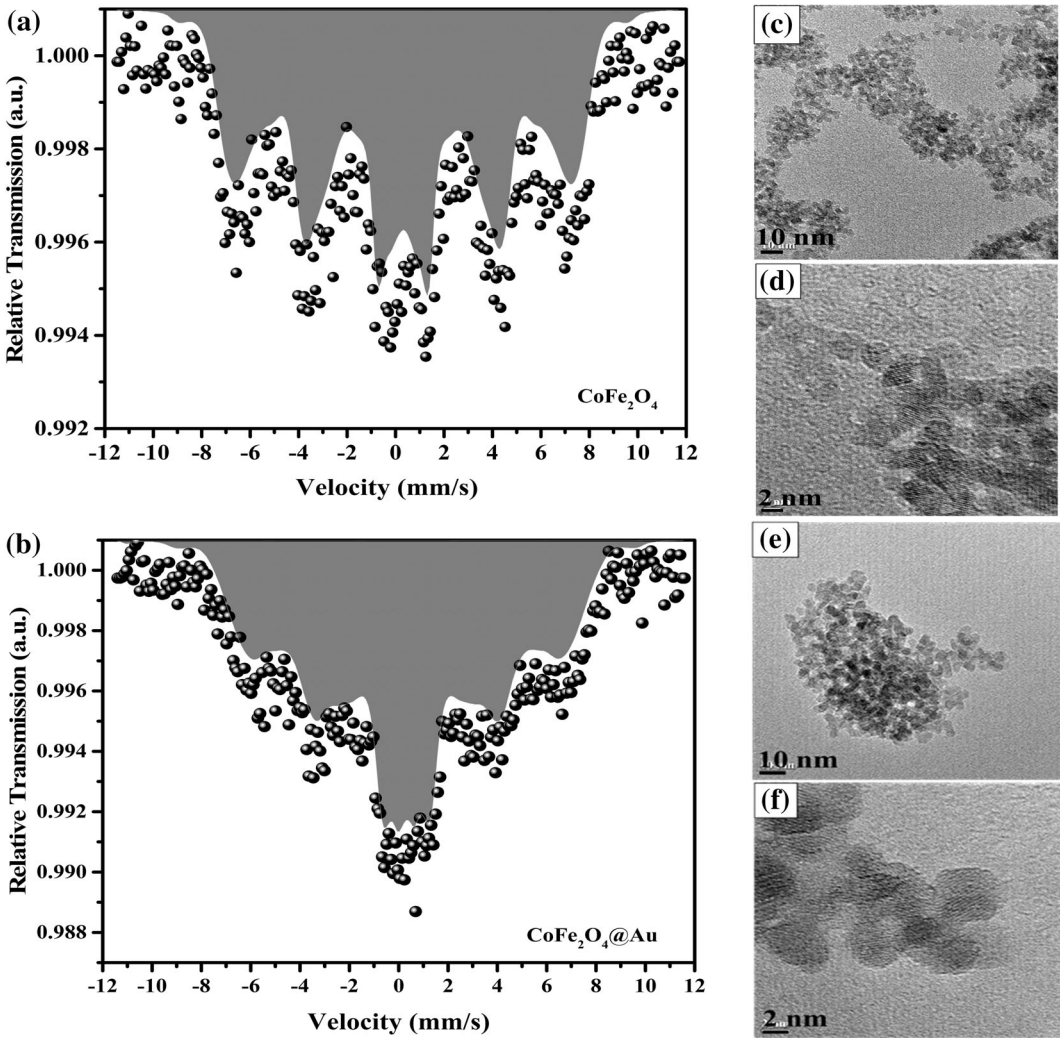

Fig. 2 Mossbauer spectra recorded at room temperature of $CoFe_2O_4$ NPs **a** and $CoFe_2O_4$@Au CSs **b**, (sphere points showing the recorded data points and the gray area showing the distribution of hyperfine field fit using NORMOS/DIST program); representative HRTEM micrographs of $CoFe_2O_4$NPs **c**, **d**, $CoFe_2O_4$@Au CSs **e**, **f**

plays a vital role in obtaining higher values of SAR. An increase in the concentration of magnetic particles resulted in an increased value of maximal ΔT, and the same trend was observed for both samples. On the other hand, increasing the concentration of magnetic nanoparticles resulted in a decrease in SAR in both cases. Therefore, it can be inferred that increasing particle concentration to achieve maximal temperature is not a solution to obtain a high value of SAR. SAR is also dependent on magnetic field, frequency, anisotropy and other physical parameters such as particle size and morphology (Table S1). The maximal value of SAR obtained in our case is 68.85 W g^{-1} for $CoFe_2O_4$ NPs and 54.97 W g^{-1} for $CoFe_2O_4$@Au CSs at a concentration of 5 mg mL^{-1} (Table 2), comparable to those reported in the literature for potential hyperthermia agents. From our results, the presence of Au does not have any pronounced effect on the SAR of $CoFe_2O_4$ NPs, and they can serve as a good coating agent for MNPs. To determine the applicability and to compare the SAR values obtained from the literature at different extrinsic conditions including magnetic field, frequency, size and concentration of MNPs, the more suitable term is used as intrinsic loss power (ILP, in $nHm^2\ kg^{-1}$) measured in nano-Henrys m^2 per kg and can be defined as [24]

$$\mathrm{ILP}\left[\mathrm{nHm^2\ kg^{-1}}\right] = \frac{\mathrm{SAR[W\ kg^{-1}]}}{f[\mathrm{kHz}]H^2[(\mathrm{kA\ m^{-1}})^2]}$$

The SAR value scales linearly with the frequency and quadratically with the amplitude of the magnetic field. Thus, ILP is the most suitable term used to define the applicability of the MNPs. The frequency and the amplitude used in the experiments are accountable to determine the ILP values. The obtained SAR values from our results were further processed using the equation to determine the

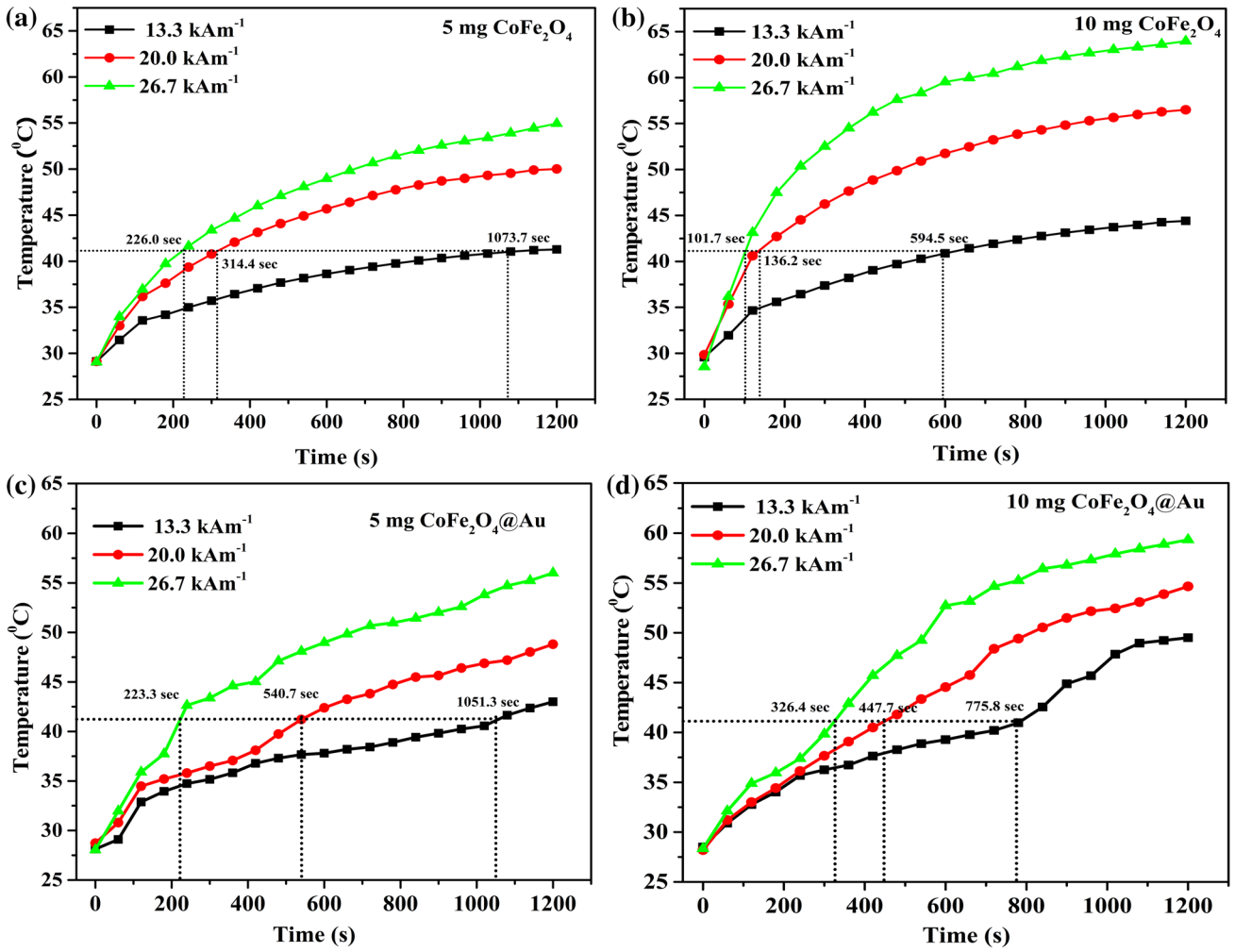

Fig. 3 Temperature–time curves of **a** 5 mg mL^{-1}; **b** 10 mg mL^{-1} $CoFe_2O_4$ MNPs; **c** 5 mg mL^{-1}; **d** 10 mg mL^{-1} $CoFe_2O_4$@Au CS at different applied AC magnetic fields (dotted line showing the threshold hyperthermia temperature at respective time in s)

Table 2 Calculated rise in temperature (ΔT, °C), specific absorption rate (SAR, W g^{-1}) and intrinsic loss power (ILP, nHm^2 kg^{-1}) of $CoFe_2O_4$ NPs and $CoFe_2O_4$@Au CSs NPs

Applied field (H) →		13.3 (kA m^{-1})			20.0 (kA m^{-1})			26.7 (kA m^{-1})		
Sample	Conc. (mg mL)	ΔT	SAR	ILP	ΔT	SAR	ILP	ΔT	SAR	ILP
$CoFe_2O_4$	5	12.16	32.81	0.67	20.88	54.26	0.49	25.89	68.85	0.35
	10	14.83	17.89	0.37	26.65	38.82	0.35	35.43	53.76	0.27
$CoFe_2O_4$@Au	5	14.88	33.38	0.68	20.08	40.32	0.37	27.94	54.97	0.28
	10	21.00	16.91	0.35	26.47	21.21	0.19	31.10	26.64	0.14

ILP values (Table 2). Our results indicated that the ILP values decreased with an increase in MNP concentration and amplitude of the magnetic field. The obtained highest value of ILP for $CoFe_2O_4$ NPs was 0.67 while that for $CoFe_2O_4$@Au CSs is 0.68 nHm^2 kg^{-1} using a 5 mg mL^{-1} MNPs concentration at 13.3 kA m^{-1} and 276 kHz of amplitude and frequency, respectively. The ILP values were also determined from the SAR of $CoFe_2O_4$ reported in the literature as bare and CSs (Table S1), and our results are comparable with the literature values. Further in vivo and in vitro study is suggested to determine the biocompatibility of synthesized CS MNPs.

4 Conclusion

We report a simple one-step synthesis method for the water-dispersible $CoFe_2O_4$ and $CoFe_2O_4$@Au CS MNPs with an average size of ~ 5 nm. The surface modification of $CoFe_2O_4$ with Au is confirmed using XRD, TEM, UV,

PL, IR and Raman spectroscopy as well as with *M–H* curves and Mossbauer techniques. The induction heating studies showed the ability of $CoFe_2O_4$@Au CS to reach the hyperthermia temperature. The highest ILP obtained in our study was 0.67 for $CoFe_2O_4$ and 0.68 $nHm^2\ kg^{-1}$ for $CoFe_2O_4$@Au using a 5 mg mL^{-1} MNPs concentration at 13.3 kA m^{-1} and 276 kHz of amplitude and frequency, respectively. However, at these extrinsic parameters, the obtained MNP samples were unable to reach the threshold hyperthermia temperature. Hence, use of both the SAR and ILP parameters to explain the efficiency of the MNPs for the hyperthermia applications is suggested. From our study, it is observed that 5 mg mL^{-1} $CoFe_2O_4$@Au CSs with 54.97 W g^{-1} of SAR and 0.28 $nHm^2\ kg^{-1}$ of ILP is suitable for the hyperthermia cancer treatment. More in vivo and in vitro studies will be conducted in order to ascertain their applications in cancer treatment.

Acknowledgements Author (Sandip Sabale) is thankful to University Grants Commission, New Delhi, India, for Raman Fellowship to work in USA (F. No. 5-105/2016 (IC), February 10, 2016. Authors are grateful to the Department of Science & Technology, New Delhi, for the grants under DST-FIST program (No. SR/FST/college-151/2013 (C)) to Jaysingpur College, Jaysingpur. Xiao-Ying Yu thanks the MS3 Initiative at the Pacific Northwest National Laboratory (PNNL) operated by Battelle for the Department of Energy. We thank Rachel Komorek for English editing.

References

[1] H. Shokrollahi, J. Magn. Mag. Mater. **426**, 74 (2017)
[2] S.M. Silva, R. Tavallaie, L. Sandiford, R.D. Tilley, J.J. Gooding, Chem. Commun. **52**(48), 7528 (2016)
[3] S. Sabale, P. Kandesar, V. Jadhav, R. Komorek, R.K. Motkuri, X.Y. Yu, Biomater. Sci. **5**(11), 2212 (2017)
[4] J.C. Li, Y. Hu, J. Yang, P. Wei, W.J. Sun, M.W. Shen, G.X. Zhang, X.Y. Shi, Biomaterials **38**, 10 (2015)
[5] W. Gao, L.F. Ji, L. Li, G.W. Cui, K.H. Xu, P. Li, B. Tang, Biomaterials **33**(14), 3710 (2012)
[6] J.H. Lee, J.T. Jang, J.S. Choi, S.H. Moon, S.H. Noh, J.W. Kim, J.G. Kim, I.S. Kim, K.I. Park, J. Cheon, Nat. Nano. **6**(7), 418 (2011)
[7] S. Sabale, V. Jadhav, V. Khot, X. Zhu, M. Xin, H. Chen, J. Mater. Sci. Mater. Med. **26**(3), 127 (2015)
[8] S. Sabale, V. Khot, V. Jadhav, X.L. Zhu, Y.H. Xu, Acta Metall. Sin. (Engl. Lett.) **27**(6), 1122 (2014)
[9] N.R. Panda, D. Sahu, B.S. Acharya, P. Nayak, S.P. Patil, D. Das, Acta Metall. Sin. (Engl. Lett.) **27**(4), 563 (2014)
[10] Y. Pineiro, Z. Vargas, J. Rivas, M.A. Lopez-Quintela, Eur. J. Inorg. Chem. **27**, 4495 (2015)
[11] N. Bachan, A. Asha, W. Jothi Jeyarani, D. Arun Kumar, J. Merline Shyla, Acta Metall. Sin. (Engl. Lett.) **28**(11), 1317 (2015)
[12] V. Revathi, S. Dinesh Kumar, P. Chithra Lekha, V. Subramanian, T.S. Natarajan, C. Muthamizhchelvan, Acta Metall. Sin. (Engl. Lett.)**27**(4), 557 (2014)
[13] H.Y. Zhao, L. Liu, J. He, C.C. Pan, H. Li, Z.Y. Zhou, Y. Ding, D. Huo, Y. Hu, Biomaterials **51**, 194 (2015)
[14] I. Robinson, L.D. Tung, S. Maenosono, C. Walti, N.T.K. Thanh, Nanoscale **2**(12), 2624 (2010)
[15] Y.M. Shao, L.C. Zhou, C. Bao, Q. Wu, W.L. Wu, M.Z. Liu, New J. Chem. **40**(11), 9684 (2016)
[16] Q.D. Xia, S.S. Fu, G.J. Ren, F. Chai, J.J. Jiang, F.Y. Qu, New J. Chem. **40**(1), 818 (2016)
[17] A. Mikalauskaite, R. Kondrotas, G. Niaura, A. Jagminas, J. Phys. Chem. C **119**(30), 17398 (2015)
[18] G.V.M. Jacintho, A.G. Brolo, P. Corio, P.A.Z. Suarez, J.C. Rubim, J. Phys. Chem. C **113**(18), 7684 (2009)
[19] G. Shemer, E. Tirosh, T. Livneh, G. Markovich, J. Phys. Chem. C **111**(39), 14334 (2007)
[20] M. Abdulla-Al-Mamun, Y. Kusumoto, T. Zannat, Y. Horie, H. Manaka, RSC Adv. **3**(21), 7816 (2013)
[21] C.X. Zhang, Q. Luo, J.H. Shi, L.Y. Yue, Z.B. Wang, X.H. Chen, S.M. Huang, Nanoscale **9**(8), 2852 (2017)
[22] P.L. Andrade, V.A.J. Silva, J.C. Maciel, M.M. Santillan, N.O. Moreno, L.D. Valladares, A. Bustamante, S.M.B. Pereira, M.P.C. Silva, J.A. Aguiar, Hyperfine Interact. **224**(1–3), 217 (2014)
[23] S. Karamipour, M.S. Sadjadi, N. Farhadyar, Spectrochim. Acta A Mol. Biomol. Spectrosc. **148**, 146 (2015)
[24] R.R. Wildeboer, P. Southern, Q.A. Pankhurst, J. Phys. D Appl. Phys. (2014). https://doi.org/10.1088/0022-3727/47/49/495003